International Journal of Thermal Sciences 82 (2014) 62–71

Contents lists available at ScienceDirect

International Journal of Thermal Sciences

journal homepage: www.elsevier.com/locate/ijts

Natural convection from rectangular interrupted fins

Mehran Ahmadi, Golnoosh Mostafavi, Majid Bahrami*

Laboratory for Alternative Energy Conversion (LAEC), Mechatronic Systems Engineering, Simon Fraser University (SFU), Surrey, BC, Canada

ARTICLE INFO

Article history:
Received 18 September 2013
Received in revised form
25 March 2014
Accepted 26 March 2014
Available online 4 May 2014

Keywords:
Heat transfer
Natural convection
Interrupted fins
Optimum gap
Experimental study
Numerical simulation

ABSTRACT

Steady-state external natural convection heat transfer from vertically-mounted rectangular interrupted fins is investigated numerically and experimentally. FLUENT software is used to develop a 2-D numerical model for investigation of fin interruption effects. A custom-designed testbed was developed and 12 different aluminum alloy heatsinks with various geometric dimensions are machined and tested to verify the theoretical results. A comprehensive experimental–numerical parametric study is performed to investigate the effects of fin spacing, and fin interruption. Our results show that adding interruptions to vertically-mounted rectangular fins can enhance the thermal performance considerably and that an optimum fin interruption exists. A new compact correlation is proposed for calculating the optimum interruption length. The results of this work can be used to improve natural heat transfer from enclosures in a variety of electronics, power electronics and telecom applications.

1. Introduction

Passive cooling is a widely preferred method for electronic, power electronic, and telecommunication devices since it is a cost effective, quiet, and reliable solution. Air-cooling is recognized as an important technique in the thermal design of electronic packages, because its accessibility particularly with respect to safe operation in hostile environments (contaminated air, vibrations, noise, and humidity) [1]. These features stimulate considerable research on the development of efficient finned heatsinks and enclosures [2–6]. Telecommunication devices are an example of electronic systems that require efficient thermal management. About one percent of global total energy consumption in year 2007 was used by telecommunication devices, which is equal to energy consumed by 15 million US homes, with equivalent CO_2 emission of 29 million cars [7]; 25% of this energy is required for cooling and thermal management of these systems [8]. Natural convective heat transfer form vertical rectangular fins and pin fins is a well-established subject in the literature. It has been investigated analytically, numerically and experimentally. The following paragraphs provide a brief overview on the pertinent literature; the previous studies are grouped into analytical, numerical, and experimental studies. More detailed reviews can be found elsewhere, see e.g. Ref. [9]. Table 1 provides a summary of the methods used, reported correlations, and major findings in the literature.

Pioneering analytical work in this area was carried out by Elenbaas [10]. He investigated isotheral finned heatsink analytically and experimentally. His analytical study resulted in general relations for natural convective heat transfer from vertical rectangular fins; which, however, was not accurate for small values of fin spacing. Churchill [11] developed a general correlation for the natural convection heat transfer rate from vertical channels using the theoretical and experimental results reported by a number of authors. Bar-Cohen and Rohsenow [12] also performed an analytical study to investigate the natural convective heat transfer from two vertical parallel plates. They developed a relationship for the Nusselt number as a function of the Rayleigh number for isothermal and isoflux plates; a correlation was reported for the optimum fin spacing.

$$Nu_s = \frac{hs}{k} = \left[\frac{576}{\left(\frac{Ra_s s}{L}\right)^2} + \frac{2.873}{\left(\frac{Ra_s s}{L}\right)^{0.5}}\right]^{-0.5} \quad (1)$$

where Ra_s is the Rayleigh number based on fin spacing, s is the fin spacing between two adjacent fins, L is the fin length, h is convective heat transfer coefficient, and k is thermal conductivity, respectively. Fig. 1 shows the geometry of the vertical heatsink schematically. Another relation was introduced by Culham et al. [13] using the squared root of the wetted area of the fins as the characteristic length scale.

Bodoia and Osterle [14] followed Elenbaas [10] and used a numerical approach to investigate the developing flow in a vertical

* Corresponding author.
E-mail addresses: mahmadi@sfu.ca, ahmadi.mehran@gmai.com (M. Ahmadi).

http://dx.doi.org/10.1016/j.ijthermalsci.2014.03.016
1290-0729/

Table 1
Literature review on natural convective heat transfer from vertical rectangular fin.

Ref.#	Method	*Ra* range	Correlation *Nu*	Condition	Notes
[18]	Analytical & experimental	10^{-1}–10^{5}	$\frac{1}{24}Ra_s\left[1-\exp\left(-\frac{35}{Ra_s}\right)\right]^{\frac{3}{4}}$	Symmetric isothermal	Reported S_{opt} as function of H
[44]	Analytical	all	$\left[\left(\frac{24}{Ra_s}\right)^2+\left(\frac{1}{0.59Ra_s^{0.25}}\right)^2\right]^{-0.5}$	Symmetric isothermal	Developing + developed flows
[31]			$\left[\left(\frac{6}{Ra_s}\right)^2+\left(\frac{1}{0.59Ra_s^{0.25}}\right)^2\right]^{-0.5}$	Asymmetric isothermal	Reported S_{opt}
[10]	Experimental & numerical		$\left[\left(\frac{12}{\frac{s}{L}Ra_s}\right)^2+\left(\frac{1}{0.619\left(\frac{s}{L}Ra_s\right)^{0.25}}\right)^2\right]^{-0.5}$	Asymmetric isothermal	Not a 3D problem, its 2D Developing + developed flows
[39]	Experimental	$s<50$ mm	$6.7\times10^{-4}Ra_s\left[1-\exp\left(\frac{7460}{Ra_s}\right)^{0.44}\right]^{1.7}$	Symmetric isothermal Horizontal	Reported $S_{\mathrm{opt}}=f(H,s)$
		$s>50$ mm	$0.54\,Ra_s^{0.25}$		
[18]	Experimental	$Ra<250$	$0.135Ra_s^{0.5}$		
		$250<Ra<10^6$	$0.423Ra_s^{\frac{1}{3}}$		
[32]	Experimental	$Ra<250$	$0.144Ra_s^{0.5}$	Small fin heights	
		$250<Ra<10^6$	$0.490Ra_s^{\frac{1}{3}}$		

and the natural convection heat transfer between symmetrically heated, isothermal plates in an effort to predict the channel length required to achieve fully developed flow as a function of the channel width and wall temperature. Ofi and Hetherington [15] used a finite element method to study the natural convective heat transfer from open vertical channels. Culham et al. [13] also developed a numerical code to simulate the free convective heat transfer from a vertical fin array.

Several experimental studies were carried out on this topic. Starner and McManus [16] Welling and Wooldridge [17], Chaddock [18], Aihara [19–22], Leung et al. [23–29] and Van de Pol and Tierney [30] are some examples, these studies were mostly focused on the effects of varying fin geometric parameters, the array, and base plate orientation.

Radiation heat transfer plays a key role in the heat transfer from fin arrays. This has been shown by Edwards and Chaddock [31], Chaddock [18], Sparrow and Acharya [32], Saikhedkar and Sukhatme [33], Sparrow and Vemuri [34,35], Azarkish et al. [36], and Rao et al. [37]. It has been reported that the radiation heat transfer contributes between 25 and 40% of the total heat transfer from fin arrays in naturally cooled heatsinks.

In spite the number of existing literature on the topic, our review indicates that the focus has been mostly on continuous fins and pin fins, and no in-depth study has been performed to investigate the natural convection heat transfer from interrupted fins for external natural convective heat transfer. As such, in this paper, we aim at investigating the effect of fin interruption on natural convection in vertical rectangular fins. The targeted geometry, i.e., interrupted fins, are more general and can cover both continuous and pin fins at the limits; please see Fig. 1. A proper selection of fin spacing and interruption gap can lead to higher heat transfer coefficients, which in turn leads to higher heat transfer rates that can extend the limits of natural cooling. Furthermore, fin interruption can lead to significant weight reduction in heatsinks and material

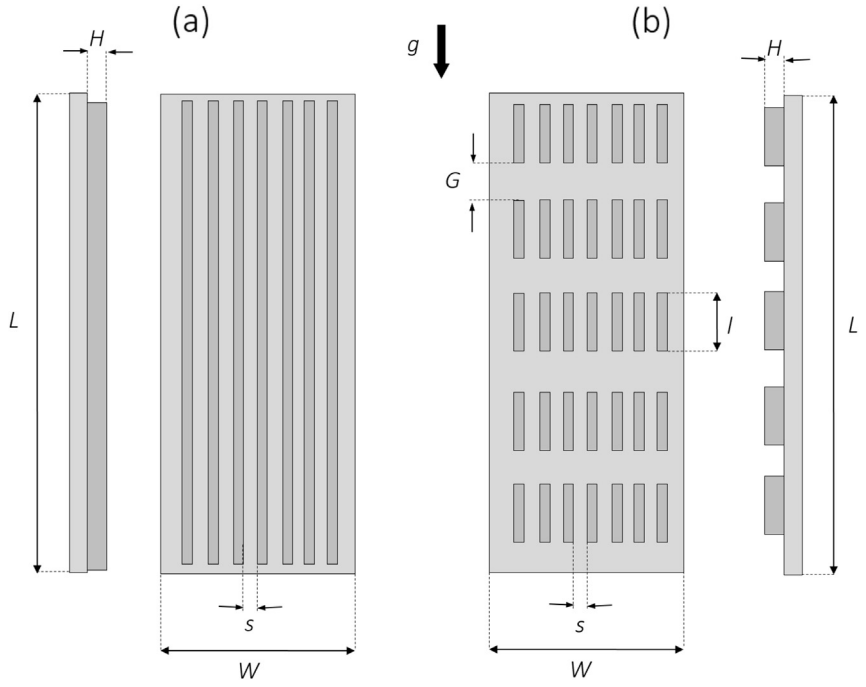

Fig. 1. Schematic of the considered heatsink geometry, a) continuous rectangular fin heatsink; b) interrupted rectangular fin heatsink.

and manufacturing cost reductions. The goal of this study is to investigate the effects of fin interruption and determining an optimum value for different geometrical parameters of vertical fin arrays, mainly the length of fin interruption. The effect of fin interruption is investigated using a 2-D numerical simulation implementing FLUENT in this study. A custom-built testbed is designed and twelve different heatsink samples are prepared and tested to validate the numerical results. A new compact correlation is developed to accurately predict the optimum fin interruption for vertically mounted rectangular fins.

2. Problem statement

A schematic of the considered fin geometry with the salient geometric parameters is shown in Fig. 1. When a heatsink is heated, the buoyancy force causes the surrounding fluid to start moving and as a result thermal boundary layers start to develop at the bottom edges of the fins; the boundary layers eventually merge if the fins/channels are sufficiently long, creating a fully developed channel flow [38]. Interrupted fins, however, disrupt the thermal boundary layer growth, maintaining a thermally developing flow regime, which can lead to a higher natural heat transfer coefficient.

To investigate the effects of fin interruption and to determine an optimum fin length to interruption ratio, we started by using the existing analytical models of [39,40] to calculate the optimum fin spacing, s. The idea is to decouple the effect of fin spacing from the fin interruption. As such, the fin spacing will be kept constant at its optimum value proposed by Rohsenow–Bar-Cohen model [39] throughout the analysis. We also independently investigated the effect of fin spacing experimentally. Our experimental results match the optimum fin spacing values reported by Ref. [39].

2.1. Governing equation and boundary conditions

The present model consists of the external natural convection heat transfer from a single channel. The conservation of mass, momentum and energy in the fluid are based on assuming a fluid with constant properties and the Boussinesq approximation [38] for density–temperature relation; Eqs. (2)–(5) summarize the governing equations.

$$\frac{\partial u}{\partial x}+\frac{\partial v}{\partial y}=0 \tag{2}$$

$$\rho\left(u\frac{\partial u}{\partial x}+v\frac{\partial u}{\partial y}\right)=-\frac{\partial P}{\partial x}+\mu\nabla^2 u \tag{3}$$

$$\rho\left(u\frac{\partial v}{\partial x}+v\frac{\partial v}{\partial y}\right)=-\frac{\partial P}{\partial y}+\mu\nabla^2 v-\rho g \tag{4}$$

$$u\frac{\partial T}{\partial x}+v\frac{\partial T}{\partial y}=\alpha\nabla^2 T \tag{5}$$

where y is the direction parallel to the gravitational acceleration and x is the direction normal to the gravitational acceleration, u is the flow velocity in x-direction and v is the flow velocity in y-direction, respectively. Here, ρ, μ and α are the fluid's density, dynamic viscosity and thermal diffusivity, respectively.

Considering $\partial P/\partial y=\partial P_\infty/\partial y$, where P_∞ is the ambient hydrostatic pressure, and assuming Boussinesq approximation, Eq. (4) yields to:

$$u\frac{\partial v}{\partial x}+v\frac{\partial v}{\partial y}=\nu\frac{\partial^2 v}{\partial x^2}+g\beta(T-T_\infty) \tag{6}$$

The governing equations are subjected to the following boundary conditions:

$$\text{At } x=0,\ 0\le y\le l+G;\quad \frac{\partial T(0,y)}{\partial x}=0 \tag{7}$$

$$\text{At } x=\pm s,\ 0\le y\le l;\quad T(\pm s,y)=T_w \tag{8}$$

$$\text{At } y=0 \text{ and } y=l;\quad P=P_\infty \tag{9}$$

Radiation heat transfer from a surface can be calculated from Eq. (10); for more detail see Rao et al. [37]:

$$Q_{\text{rad}}=\sigma\varepsilon\left(T_w^4-T_\infty^4\right)\sum_{i=1}^{3}A_iF_{i4} \tag{10}$$

where F is the surface view factor, ε is the surface emissivity coefficient, and σ is the Stefan–Boltzmann constant equals to 5.67×10^{-8} W/m^2 K^4, respectively.

2.2. Numerical modeling

A steady state 2-D model was developed in FLUENT. Because of symmetry, a single channel, shown in Fig. 2, is chosen to represent the computational domain. According to flow visualization and velocity measurement of the flow field for a finned plate, reported in Ref. [41], the fresh air inflow and outflow in the direction normal to the base plate is negligible compared to the flow parallel to base plate, which justifies a 2-D flow hypothesis. Additionally, the effect of the two side-fins exposed to the ambient is not expected to be significant (small area), and consequently, the selection of a single channel for the numerical solution domain instead of the whole heatsink is a reasonable assumption. For the domain dimensions, the optimum fin spacing, s, is used based on the models of [12,40]. In other word, the effect of fin spacing is decoupled in simulations of interrupted fins by keeping the fin spacing constant at its optimum value. The "pressure inlet" boundary condition is applied to the channel inlet, i.e., the bottom of the channel, which defines the static gauge pressure at the inlet boundary. This is interpreted as the static pressure of the environment from which the flow enters the channel. For the top of the outlet, "pressure outlet is considered. The "symmetry" boundary condition was chosen for the centerline of interruption region, which is equivalent to "no heat flux" in the direction normal to the boundary. Also "no-slip" and "isothermal solid surface" are considered for the walls boundary condition. Fig. 2 shows a schematic of the domain considered for the numerical simulation, along with the chosen boundary conditions for continuous and interrupted fins.

To solve the system of partial differential equations, ANSYS-FLUENT 12.1.4 is employed. GAMBIT is used for mesh generation. Boundary layer mesh is used for the regions close to the fin surface; this is to capture the flow behavior with a higher resolution. A grid independency study is performed for a continuous fin case, with seven different grid sizes in the y-direction parallel to fins, and four different grid sizes in the x-direction normal to fins, see Fig. 3. The optimum size for vertical grids has chosen to be 1 mm. Also 50 grids are used in the horizontal space between the two fin surfaces.

Table 2 shows the specifications of the numerical domain geometry. Fin length and the interruption length are chosen to be $l=t$, $2t$, $5t$, $10t$, and $15t$, where t is the fin thickness. Various values are used for the interruption length as well, including: $G=l/2$, l, $2l$, $5l$, $10l$ and in some cases $20l$, $40l$, $80l$ and $225l$. Thirty six different geometries are investigated overall.

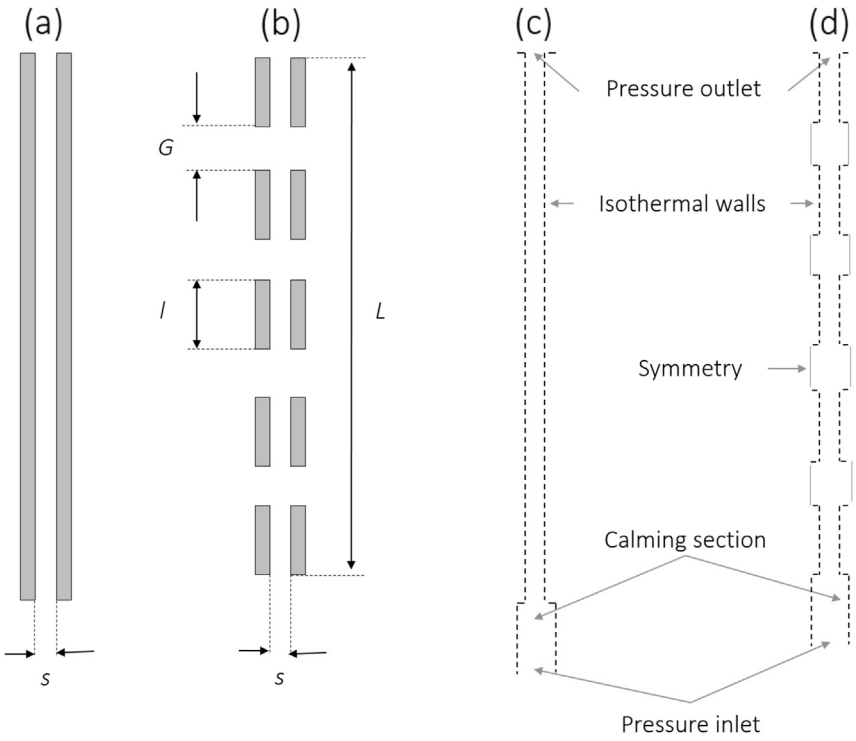

Fig. 2. Schematic of the numerical domain, a) continuous fins, b) interrupted fins; c) boundary conditions for continuous fins, d) boundary conditions for interrupted fins.

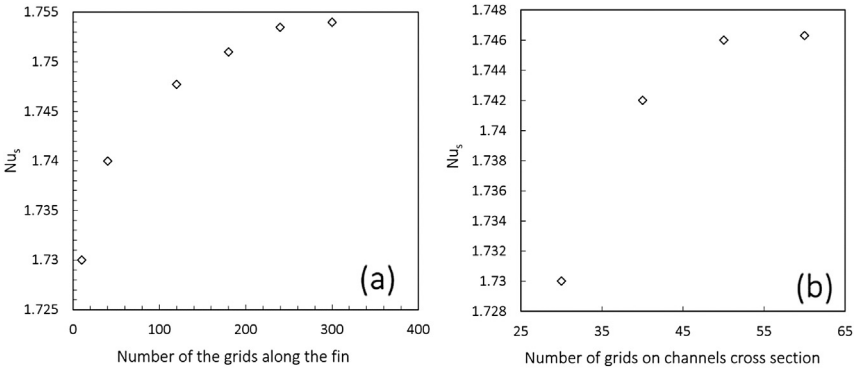

Fig. 3. Grid independency study, $Ra = 1.6E3$; a) in vertical direction (horizontal grids = 50), b) in horizontal direction (vertical grids = 300).

2.3. Experimental study

The objective of the experimental work is to verify the present numerical simulations, and also to independently investigate the effects of fin spacing and fin interruption length in vertically-mounted rectangular fins. As such, two sets of heatsink samples were prepared and tested featuring: i) continuous and ii) interrupted rectangular fins. Base plate dimensions for the samples are kept the same for all samples. The heatsinks are machined with different fin spacing and interruption length as listed in Tables 3 and 4. Twelve different samples are used to perform the experiments.

Table 2
Geometrical dimensions of the considered interrupted fins in the present numerical analysis.

Considered numerical geometry, case number	G/l	t (mm)	s (mm)
1–5	0.5	2.5	9.5
6–10	1	2.5	9.5
11–15	2	2.5	9.5
16–20	5	2.5	9.5
21–25	10	2.5	9.5
26–28	20	2.5	9.5
29–32	40	2.5	9.5
33–35	80	2.5	9.5
36	255	2.5	9.5

Fin length and fin width is constant in all the geometries, $L = 1.4$ m and $s = 9.5$ mm.

Table 3
Dimensions of heatsink samples; continuous fins, see Fig. 1a.

Sample name	s (mm)	N	H (mm)	l (mm)
Cont-1-10-17	9.5	8	17	–
Cont-1-6-17	6.0	12	17	–
Cont-1-14-17	14.0	6	17	–
Cont-1-10-10	9.5	8	10	–
Cont-1-10-25	9.5	8	25	–

Table 4
Dimensions of heatsink samples; interrupted fins, see Fig. 1b.

Sample name	s (mm)	N	H (mm)	l (mm)	n (number of interruptions)	G (mm)
Int-1-20	9.5	8	17.4	142.5	1	20
Int-2-20	9.5	8	17.4	88.3	2	20
Int-3-20	9.5	8	17.4	61.3	3	20
Int-4-20	9.5	8	17.4	45.0	4	20
Int-5-20	9.5	8	17.4	34.2	5	20
Int-4-20	9.5	8	17.4	37.0	4	30
Int-4-20	9.5	8	17.4	29.0	4	40

Fin base length and width are constant in all the samples, $L = 305$ mm and $W = 101$ mm.

2.3.1. Testbed

The tested heatsinks are machined from 6063-T5 aluminum alloy with a thermal conductivity of 130 W/m K and emissivity of 0.09 at 20 °C. A new custom-made testbed is designed for measuring natural convection heat transfer from heatsinks as shown in Fig. 4. The set-up includes an enclosure made of Poly Methyl Methacrylate (PMMA) which is insulated by a layer of dense insulation foam with thickness of 15 mm. During the experiments, in addition to the power input to the electric heater, surface temperatures are measured at various locations at the back of the baseplate. Electrical power is supplied through an AC power supply (Transformer 10C) from Superior Electric (Ohio, US). The voltage and the current are measured to determine the power input to the heater. Five self-adhesive T-type copper-constantan thermocouples with accuracy of ±0.1 °C are installed in various locations on the surface of the enclosures, see Fig. 4. All thermocouples are adhered to the back side of the heatsink to prevent disturbing the buoyancy-driven air flow. An additional thermocouple is used to measure the ambient temperature during the experiments. Thermocouples are plugged into an NI 9213 Thermocouple DAQ system. Thermal paste is used to minimize the thermal contact resistance between the heater and the base plate. Temperature measurements are performed at five different vertical positions in order to monitor the temperature variation over the heatsink. The average of these five readings is taken as the base plate mean temperature. Since fins height is short, maximum fin height is 25 mm, fins are assumed to be isothermal. After powering the heater, we allow the system to reach a steady-state condition for each power input level, and then temperatures and power are recorded. The steady-state condition is ensured by monitoring the rate of changes in all thermocouples. For each of the twelve heatsinks, the experimental procedure is repeated for five different power inputs; 16, 25, 36, 42.2 and 49 W. Recording the temperature values in time, the point where the temperature difference in a 10 min time period became less than the accuracy range of the thermocouples, were considered as steady state conditions.

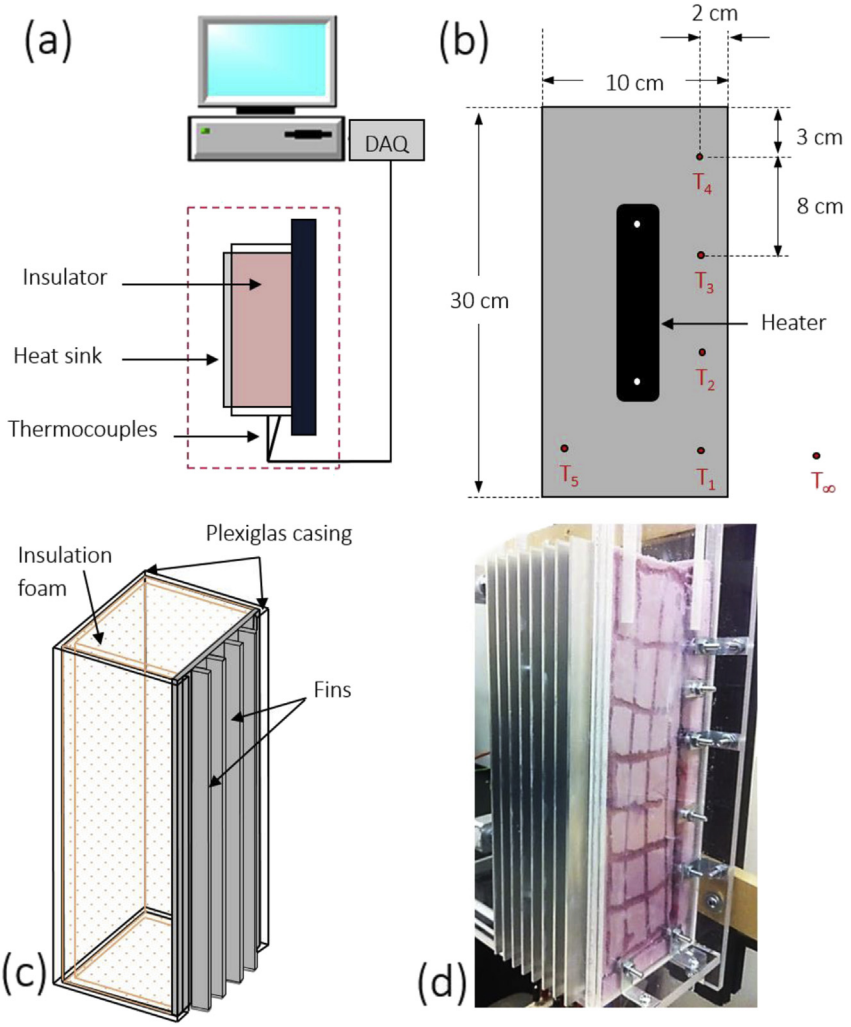

Fig. 4. Custom-made natural convection heat transfer testbed.

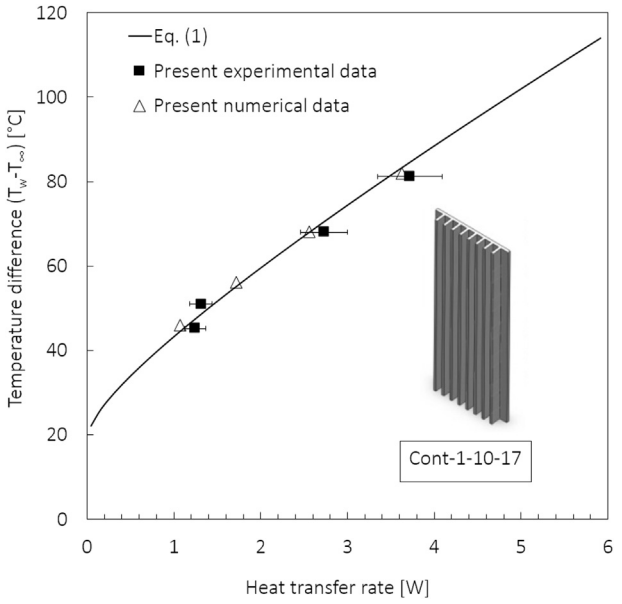

Fig. 5. Numerical simulation validation; continuous fins, single channel (s = 9.5 mm, L = 305 mm, H = 17 mm).

2.3.2. Uncertainty analysis

As given by Eq. (11), voltage and current are the electrical parameters measured in our experiments. The total accuracy in our measurements is evaluated according to the accuracy of the instruments. The accuracy of voltage and current readings are 0.5% V and 3% A (Extech® 430 multimeter), respectively. The mentioned accuracy values are given with respect to the instruments readings, and not the maximum value of the readings. The maximum uncertainty for the measurements can be calculated as follows [42]:

$$P_{\text{input}}[W] = V \cdot I \tag{11}$$

$$\omega_R = \left[\sum \left(\frac{\partial R}{\partial x_i}\omega_i\right)^2\right]^{\frac{1}{2}} \tag{12}$$

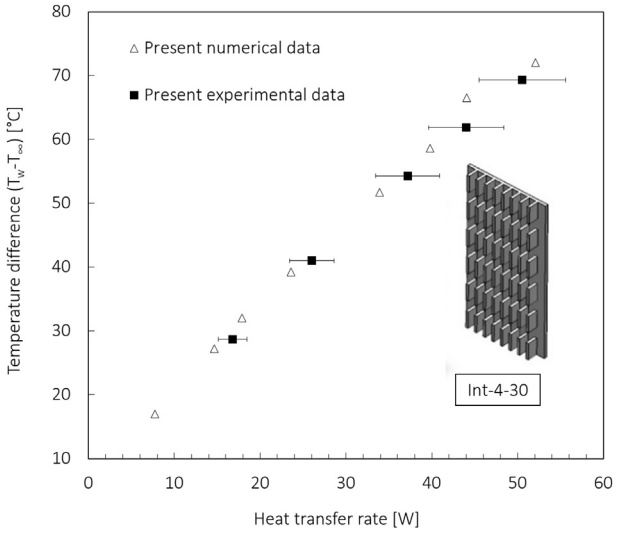

Fig. 6. Numerical simulation validation; interrupted fins (n = 8, s = 9.5 mm, L = 305 mm, H = 17 mm, l = 37 mm, G = 30 mm).

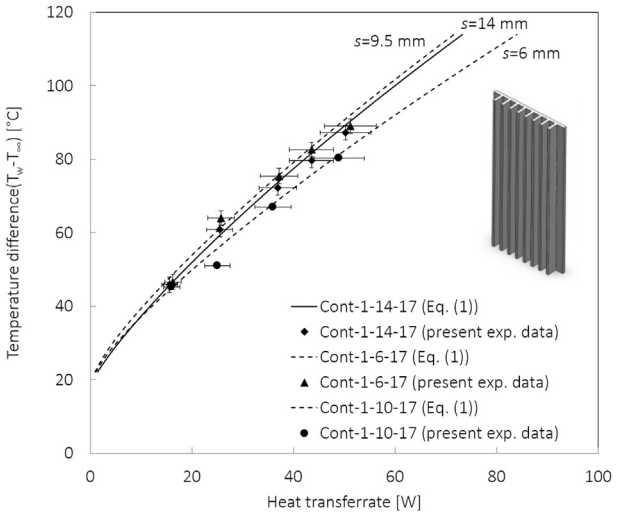

Fig. 7. Comparison of the experimental data with theoretical predictions for different fin spacing, continuous fin heatsinks.

where ω_R is the uncertainty in results $R(x_1, x_2 \ldots x_n)$, and ω_i is the uncertainty of the independent variable x_i. The final form of the uncertainty for the input power becomes;

$$\frac{\delta P_{\text{input}}}{P_{\text{input}}} = \left[\left(\frac{\delta V}{V}\right)^2 + \left(\frac{\delta I}{I}\right)^2\right]^{\frac{1}{2}} \tag{13}$$

$$\frac{\delta \dot{Q}_{\text{Rad.}}}{\dot{Q}_{\text{Rad.}}} = \left[4\left(\frac{\delta T_w}{T_w}\right)^2 + 4\left(\frac{\delta T_\infty}{T_\infty}\right)^2 + \left(\frac{\delta l}{l}\right)^2 + \left(\frac{\delta H}{H}\right)^2 + \left(\frac{\delta t}{t}\right)^2\right]^{\frac{1}{2}} \tag{14}$$

$$\dot{Q}_{N.C.}\,[W] = P_{\text{input}} + \dot{Q}_R \tag{15}$$

The uncertainty in measuring fin height or fin length is considerably smaller than that r caused by temperature measurement and it is neglected. The maximum uncertainty value is

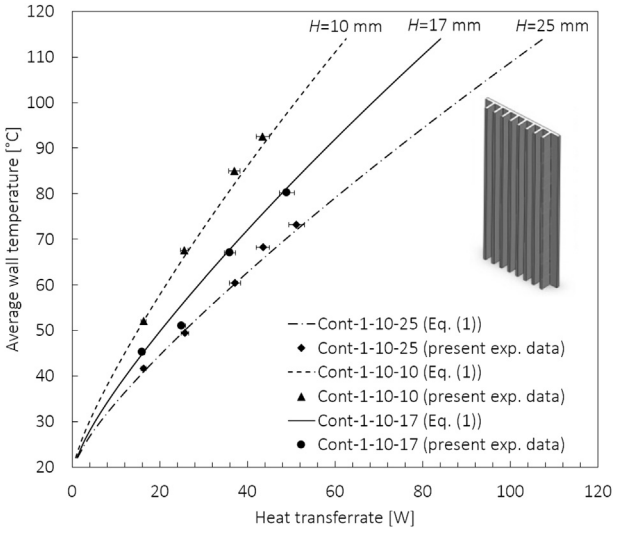

Fig. 8. Comparison of the experimental data with theoretical predictions [18] for different fin heights, continuous fin heatsinks.

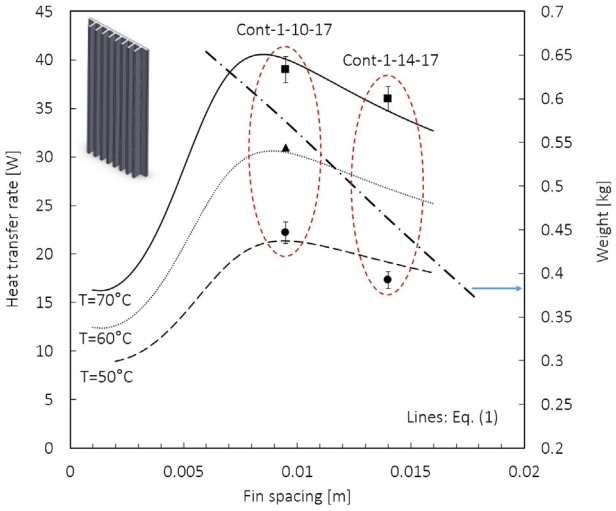

Fig. 9. Heat transfer rate versus fin spacing for different average surface temperatures, continuous fins, fin base lengths, $L = 305$ mm, heights, $H = 17$ mm.

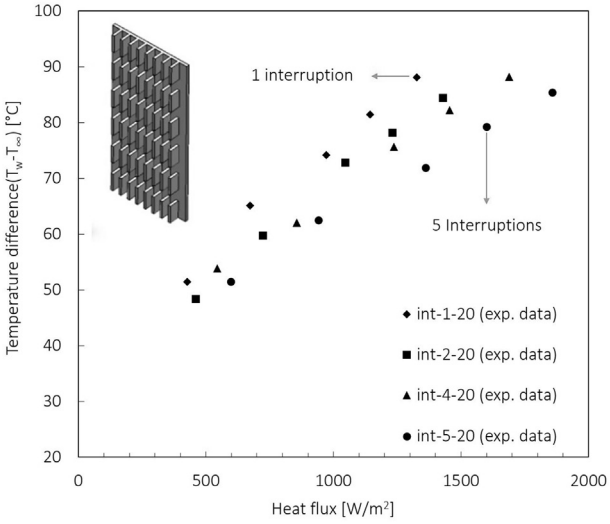

Fig. 11. Experimental data for different number of interruptions (1, 2, 3, 4, and 5), $G = 20$ mm, interrupted finned heatsinks.

calculated to be approximately 10%. The calculated uncertainties are shown as error bars in the experimental results.

Temperature difference uncertainty is only ±2 °C which is twice as the precision of the thermocouples. It should be noted that the error bars for temperature measurement uncertainty are shown in related figures, however; they are not visible since they are relatively small compared to the uncertainty of input power.

Fig. 5 shows the validation of the present numerical simulation. The simulation results for one continuous heatsink (Cont-1-10-17) are compared with our experimental data and the analytical model of [12]. As previously mentioned, the radiation is deduced from the experimental data analytically based on the average wall temperature read from the thermocouples. The emissivity was considered 0.09 for commercial aluminum [43], Prandtl number equal to 0.7, air thermal conductivity, k equal to 0.026. Natural convective heat transfer is calculated, after deducting the base plate heat transfer and radiation from the data. Figs. 5 and 6 show the results for both continuous and interrupted fins. As shown, there is a good agreement between the numerical simulation results and experimental data with a mean relative difference 4.6% and the maximum relative difference of 14%. Also the model of [12] is compared against our numerical and experimental data in Fig. 5 with a good agreement.

In Figs. 5 and 6, the measured temperatures are averaged to calculate a wall temperature for the heatsinks. Also, the convective heat transfer from the base plate (interrupted fins) is calculated using an analytical relations for flat vertical isothermal plates, Eq. (16) from Ref. [44], and deducted from the total heat transfer rates, to only consider the heat transfer from the fins. In addition, the radiation heat transfer is calculated using Eq. (10) and deducted from the data.

$$Nu_L = \left\{0.825 + \frac{0.387\, Ra_L^{\frac{1}{6}}}{\left[1 + \left(\frac{0.492}{Pr}\right)^{\frac{9}{16}}\right]^{\frac{8}{27}}}\right\}^2 \tag{16}$$

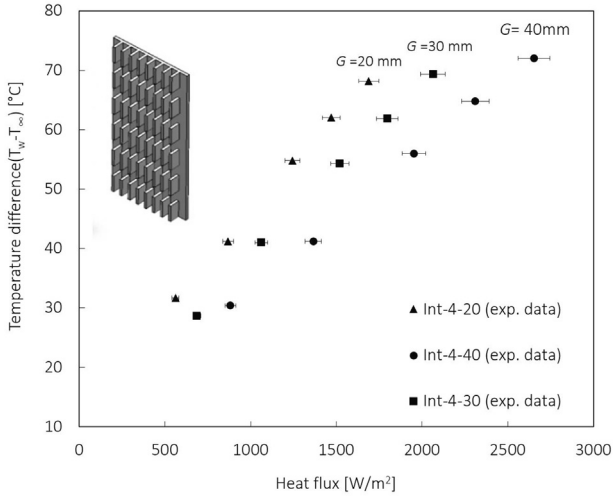

Fig. 10. Experimental data for different interruption lengths (20, 30, and 40 mm), $n = 4$, interrupted finned heatsinks.

3. Parametric study

In this section, a comprehensive parametric study is performed to investigate the effect of each heatsink parameter on natural convection heat transfer. For each case, a wide range of the targeted fin array parameter is considered, while the other geometric parameters are kept constant.

Subsequently, for the case of interrupted fins, 6 different interrupted fin heatsinks with different interruption length values are studied experimentally. After validation with experimental data, our numerical simulation is used to extend the range of interruption length, G. The results are discussed in detail in the following sections.

3.1. Effect of fin spacing

In the experimental study, 5 different continuous fin heatsinks are tested and the results are compared to the analytical existing model of [12], Eq. (1). Heat transfer rates from heatsinks are plotted as a function of average wall temperature, for fin length $L = 305$ mm, fin spacing, $s = 6.0$, 9.5 and 14.0 mm, and fin height $H = 10$, 17, and 25 mm in Figs. 7 and 8. Note that the radiation heat transfer is added to the existing analytical solutions, and the total heat transfer rates are shown in Figs. 7 and 8. As expected, the heat transfer rate from heatsinks strongly depends on the fin height, fin

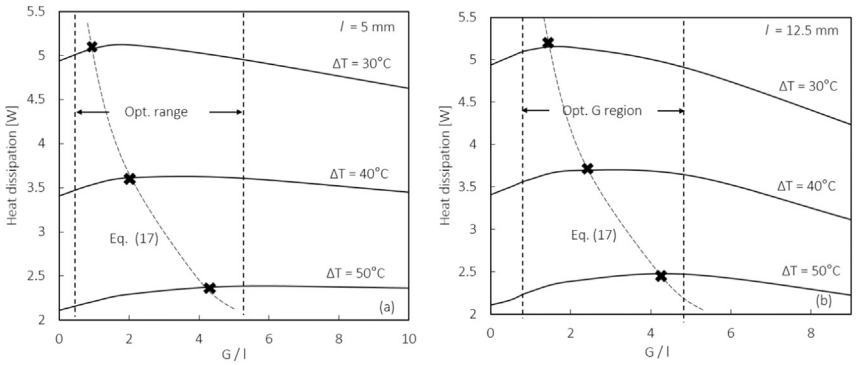

Fig. 12. Effect of interruption length on total natural convection heat transfer per number of fins, from the heatsink (numerical results), a) fin length $l = 5$ mm, b) fin length $l = 12.5$ mm.

spacing and wall temperature. It increases with an increase in the fin height and wall temperature. As shown, the experimental data and analytical solution of [12] are in good agreement with a mean relative difference of 4.6% and the maximum relative difference of 14%.

Heat transfer rate and the heatsinks mass are plotted as a function of fin spacing in Fig. 9. Fig. 9 is prepared for fin length $L = 305$ mm, fin height $H = 17$ mm and fin spacing, $s = 6$, 9.5, and 14 mm, while the heater power input is kept constant at $P_{input} = 40$ W. As shown in Fig. 9, there is an optimum fin spacing at which the heat transfer rate is maximized for different average surface temperatures. It should also be noted that the present experimental data are in good agreement when compared against the analytical and experimental results reported by Bar-Cohen and Rohsenow [12] and Tamayol and Bahrami [40], for optimum fin spacing with a mean relative difference 4.6% and maximum relative difference 14%.

3.2. Effects of fin interruption

Heat flux from heatsinks with interrupted fins is plotted in Figs. 10 and 11, as a function of average wall temperature for fin length $L = 305$ mm, fin spacing $s = 9.5$ mm, and fin height $H = 17$ mm. Fig. 10 shows the effect of interruption length. In this case four interruptions are made along the fin array and the interruption length is varied for $G = 20$, 30 and 40 mm. As expected, heat flux increases as the interruption length, G, is increased. In Fig. 11 the effect of number of interruptions is investigated; the interruption length is kept constant at 20 mm, and 1, 2, 3, 4, and 5 interruptions are added to the fins respectively. As shown, increasing the number of interruptions increases the heat flux, which is a result of frequent thermal boundary layer resets, imposed by adding the interruptions.

The effect of interruption on heat transfer enhancement can be justified by its effect on thermal and hydrodynamic boundary layers. Considering two rows of vertically aligned fins, the air flow leaves the channels formed by the lower row, with zero velocity and maximum temperature on the wall, and maximum velocity and minimum temperature on the centerline. Inside the gap region, as the air moves along the gap, the velocity and temperature profiles will become more and more evenly distributed across the gap, through a two dimensional momentum and thermal energy diffusion. Consequently the fluid reaches the upper row of fins with higher velocity and lower temperature in the region closer to the walls. This phenomena causes the thickness of both thermal and hydrodynamic boundary layers to decrease and as a result, the heat dissipation from the upper fins will increase.

Fig. 12 shows the results of numerical simulation for the effect of fin interruption on the heat transfer per number of fins. The interruption gap is started from zero, which represents a continuous fin. As shown in Fig. 12, over a certain range of interruption lengths, interrupted fins are able to enhance heat transfer in comparison with continuous fins, i.e., $G = 0$. Also there is an optimum interruption length that maximizes the total heat transfer rate from the heatsink.

There are two competing trends when interruptions are added: i) the increase in the heat flux due to the fin interruption (interrupting thermal boundary layer) and ii) the lower heat transfer surface area resulting from partial surface area removal which clearly indicates the existence of an optimum fin interruption length. This optimum interruption length is a function of surface temperature and fin length, thus, it can be correlated for different

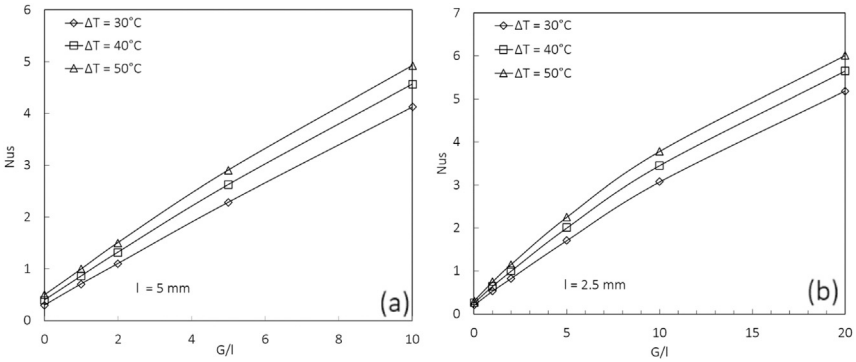

Fig. 13. Effect of interruption length on the Nusselt number for natural convection heat transfer from the fins, (numerical results), a) fin length $l = 12.5$ mm, b) fin length $l = 2.5$ mm.

lengths and fin surface temperatures. In this study, a new correlation for the optimum fin interruption, G, is presented for the range of fin length between 2.5 mm $< l <$ 25 mm:

$$\left(\frac{G}{l}\right)_{\text{opt}} = 11\left(\frac{T_w - T_\infty}{T_\infty}\right)^{-2.2} \quad (17)$$

The range of validity of Eq. (17) is $10^2 \leq Ra_s \leq 10^6$. This range is recommended based on the range Rayleigh number in our experimental and numerical studies. The proposed correlation successfully predicts the maximum heat transfer rate per number of fins for interrupted fins as shown in Fig. 12. The numerical results for interrupted fins with different G/l values in terms of Nusselt number is also shown in Fig. 13.

4. Conclusion and summary

The effects of interruptions on vertically-mounted rectangular heatsinks were studied numerically and experimentally. The interruptions will increase the heat transfer rate by resetting/interrupting the thermal and hydrodynamic boundary layers. A new custom-made testbed was built and 12 heatsink samples were machined and tested for validation the present numerical study. Our experimental and numerical results showed an increase in heat flux from the heatsink when interruptions were added. Through performing a parametric study, it was shown that an optimum interruption length exists that maximized the heat transfer from vertically-mounted rectangular heatsink. A new compact correlation was developed to calculate the optimum fin interruption for the targeted rectangular heatsinks.

Acknowledgment

This project was partially funded by “Natural Sciences and Engineering Research Council of Canada” (NSERC) and “ Mathematics of Information Technology and Complex Systems” (MITACS) which is highly appreciated by the authors. Authors would also like to acknowledge Analytic System Ware (ASW) Company for providing the heatsink samples and helpful feedbacks during the project.

Nomenclature

A	surface area, [m^2]
g	gravitational acceleration, [m/s^2]
G	fin interruption length, [m]
h	convection heat transfer coefficient, [W/m^2 K]
H	fin height, [m]
I	electrical current, [A]
k	thermal conductivity, [W/m K]
l	fin length, [m]
L	enclosure length, [m]
n	number of interruptions
N	number of fins per row
Nu	Nusselt number
P	pressure, [Pa]
P_{input}	input power, [W]
Pr	Prandtl number
Q	heat transfer rate, [W]
Ra	Rayleigh number
s	fin spacing, [m]
t	fin thickness, [m]
T	temperature, [K]
u	flow velocity in x direction, [m/s]
v	flow velocity in y direction, [m/s]
V	electrical voltage, [V]
W	enclosure width, [m]
x	direction normal to fin surface, [m]
y	direction along fin surface, [m]

Greek symbols

α	thermal diffusivity, [m^2/s]
β	coefficient of volume expansion, [1/K]
μ	fluid viscosity, [kg/m s]
ρ	density, [kg/m^3]

Subscripts

N.C.	Natural Convection
opt	optimum
R	radiation
W	wall properties
∞	ambient properties

References

[1] R.C. Chu, R.E. Simons, Recent development of computer cooling technology, in: Int. Symp. Transp. Phenom. Therm. Eng., 1993, pp. 17–25.
[2] A. Güvenç, H. Yüncü, An experimental investigation on performance of fins on a horizontal base in free convection heat transfer, J. Heat Mass Transfer 37 (2001) 409–416.
[3] B. Yazicioğlu, H. Yüncü, Optimum fin spacing of rectangular fins on a vertical base in free convection heat transfer, J. Heat Mass Transfer 44 (2006) 11–21.
[4] H. Yüncü, G. Anbar, An experimental investigation on performance of rectangular fins on a horizontal base in free convection heat transfer, J. Heat Mass Transfer 33 (1998) 507–534.
[5] M. Mobedi, H. Yüncü, A three dimensional numerical study on natural convection heat transfer from short horizontal rectangular fin array, J. Heat Mass Transfer 39 (2003) 267–275.
[6] M. Mobedi, H. Yüncü, B. Yücel, Natural convection heat transfer from horizontal rectangular fin arrays, J. Heat Transfer 89 (1967) 32–38.
[7] S.N. Roy, Energy logic: a road map to reducing energy consumption in telecommunications networks, in: INTELEC 2008-2008 IEEE 30th Int. Telecommun. Energy Conf., 2008, pp. 1–9.
[8] D.C. Kilper, S. Member, G. Atkinson, S.K. Korotky, S. Goyal, P. Vetter, et al., Power Trends Commun. Networks 17 (2011) 275–284.
[9] S. Anandan, V. Ramalingam, Thermal management of electronics: a review of literature, Therm. Sci. 12 (2008) 5–26.
[10] W. Elenbaas, Heat dissipation of parallel plates by free convection, Physica 9 (1942) 1–28.
[11] Stuart W. Churchill, A comprehensive correlation equation for buoyancy induced flow in channels, Lett. Heat Mass Transfer 4 (1977) 193–199.
[12] A. Bar-Cohen, W.M. Rohsenow, Thermally optimum spacing of vertical natural convection cooled parallel plates, Trans. ASME 106 (1984) 116–123.
[13] J.R. Culham, M.M. Yovanovich, S. Lee, Thermal modeling of isothermal cuboids and rectangular heat sinks cooled by natural convection, IEEE Trans. Compon. Packag. Manuf. Technol. Part A 18 (1995) 559–566.
[14] J.R. Bodoia, J.F. Osterle, The development of free convection between heated vertical plates, J. Heat Transfer 84 (1962) 40.
[15] O. Ofi, H.J. Hetherington, Application of the finite element method to natural convection heat transfer from the open vertical channel, Int. J. Heat Mass Transfer 20 (1977) 1195–1204.
[16] K.E. Starner, H.N. McManus, An experimental investigation of free-convection heat transfer from rectangular-fin arrays, J. Heat Transfer 85 (1963) 273–275.
[17] J.R. Welling, C.B. Wooldridge, Free convection heat transfer coefficients from rectangular vertical fins, J. Heat Transfer 87 (1965) 439.
[18] J. Chaddock, Free convection heat transfer from vertical rectangular fin arrays, ASHRAE J. (1970) 53–60.
[19] T. Aihara, Natural convection heat transfer from vertical rectangular fin arrays: (part 3, heat transfer from fin flats), Trans. Jpn. Soc. Mech. Eng. 13 (1970) 1192–1200.
[20] T. Aihara, Natural convection heat transfer from vertical rectangular fin arrays: (part 2, heat transfer from fin edges), Trans. Jpn. Soc. Mech. Eng. 36 (1970) 239–247.
[21] T. Aihara, Natural convection heat transfer from vertical rectangular fin arrays: (part 1, heat transfer from base plates), Trans. Jpn. Soc. Mech. Eng. 34 (1968) 915–926.
[22] T. Aihara, Natural convection heat transfer from vertical rectangular-fin arrays: part 4, heat-transfer characteristics of nonisothermal-fin arrays, Trans. Jpn. Soc. Mech. Eng. 36 (1970) 2077–2086.
[23] C.W. Leung, S.D. Probert, Heat exchanger: optimal separation for vertical rectangular fins protruding from vertical rectangular base, Appl. Energy 19 (1985) 77–85.
[24] C.W. Leung, S.D. Probert, M.J. Shilston, Heat exchanger design: optimal uniform separation between rectangular fins protruding from a vertical rectangular base, Appl. Energy 19 (1985) 287–299.

[25] C. Leung, S. Probert, M. Shilston, Heat exchanger design: thermal performances of rectangular fins protruding from vertical or horizontal rectangular bases, Appl. Energy 20 (2) (1985) 123–140.
[26] C. Leung, S. Probert, M. Shilston, Heat transfer performances of vertical rectangular fins protruding from rectangular bases: effect of fin length, Appl. Energy 22 (4) (1986) 313–318.
[27] C.W. Leung, S.D. Probert, Natural-convective heat exchanger with vertical rectangular fins and base: design criteria, in: Proc. Inst. Mech. Eng. Part C J. Mech. Eng. Sci., 201, 1987, pp. 365–372.
[28] C.W. Leung, S.D. Probert, Heat-exchanger performance: effect of orientation, Appl. Energy 33 (1989) 235–252.
[29] C.W. Leung, S.D. Probert, Thermal effectiveness of short-protrusion rectangular heat exchanger fins, J. Appl. Energy 34 (1989) 1–8.
[30] D. Van de Pol, J. Tierney, Free convection heat transfer from vertical fin-arrays, Parts, Hybrids, Packag. IEEE 10 (1974) 267–271.
[31] J. Edwards, J. Chaddock, An experimental investigation of the radiation and free convection heat transfer from a cylindrical disk extended surface, ASHRAE Trans. 69 (1963) 313–322.
[32] E.M. Sparrow, S. Acharya, A natural convection fin with a solution-determined nonmonotonically varying heat transfer coefficient, J. Heat Transfer 103 (1981) 218–226.
[33] N.H. Saikhedkar, S.P. Sukhatme, Heat transfer from rectangular cross-sectioned vertical fin arrays, in: Proc. Sixth Natl. Heat Mass Transfer Conf. HMT, 1981, pp. 9–81.
[34] E.M. Sparrow, S.B. Vemuri, Natural convection/radiation heat transfer from highly populated pin fin arrays, J. Heat Transfer. 107 (n.d.) (1981) 190–197.
[35] E.M. Sparrow, S.B. Vemuri, Orientation effects on natural convection/radiation heat transfer from pin-fin arrays, Int. J. Heat Mass Transfer 29 (1986) 359–368.
[36] H. Azarkish, S.M.H. Sarvari, A. Behzadmehr, Optimum geometry design of a longitudinal fin with volumetric heat generation under the influences of natural convection and radiation, Energy Convers. Manag. 51 (2010) 1938–1946.
[37] V.D. Rao, S.V. Naidu, B.G. Rao, K.V. Sharma, Heat transfer from a horizontal fin array by natural convection and radiation—A conjugate analysis, Int. J. Heat Mass Transfer 49 (2006) 3379–3391.
[38] A. Bejan, Convection Heat Transfer, third ed., John Wiley and Sons, Inc., New York, 2004.
[39] A. Bar-Cohen, W.M. Rohsenow, Thermally optimum spacing of vertical, natural convection cooled, parallel plates, J. Heat Transfer 106 (1984) 116–123.
[40] A. Tamayol, M. Bahrami, Assessment of thermal performance of electronic enclosures with rectangular fins: a passive thermal solution, in: Proc. ASME Pacific Rim Tech. Conf. Expo. Packag. Integr. Electron. Photonic Syst., InterPACK, Portland, 2011, pp. 1–8.
[41] T. Aihara, S. Maruyama, S. Kobayakawa, Free convective/radiative heat transfer from pin-fin arrays with a vertical base plate (general representation of heat transfer performance), Int. J. Heat Mass Transfer 33 (1990) 1223–1232.
[42] J.R. Taylor, An Introduction to Error Analysis: the Study of Uncertainties in Physical Measurements, second ed., University Science Books, Sausalito, California, 1997.
[43] J.P. Holman, Heat Transfer, tenth ed., McGraw Hill, Boston, 2010.
[44] S.W. Churchill, H. Chu, Correlating equations for laminar and turbulent free convection from a vertical plate, Int. J. Heat Mass Transfer 18 (1975) 1323–1329.